Sensors and Actuators A 266 (2017) 232–241

Contents lists available at ScienceDirect

Sensors and Actuators A: Physical

journal homepage: www.elsevier.com/locate/sna

High temperature gradient calorimetric wall shear stress micro-sensor for flow separation detection

Cécile Ghouila-Houri[a,b,*], Quentin Gallas[b], Eric Garnier[b], Alain Merlen[a,b], Romain Viard[c], Abdelkrim Talbi[a], Philippe Pernod[a]

[a] Univ. Lille, CNRS, Centrale Lille, ISEN, Univ. Valenciennes, UMR 8520—IEMN, LIA LICS/LEMAC, F-59000 Lille, France
[b] ONERA, Chemin de la Hunière 91123, Palaiseau, France
[c] Fluiditech, Thurmelec, 68840, Pulversheim, France

ARTICLE INFO

Article history:
Received 13 July 2017
Received in revised form
14 September 2017
Accepted 18 September 2017
Available online 19 September 2017

Keywords:
MEMS sensors
Wall shear-stress sensor
Flow separation detection
Flow control

ABSTRACT

The paper describes and discusses the design and testing of an efficient and high-sensitivity calorimetric thermal sensor developed for bi-directional wall shear stress measurements in aerodynamic flows. The main technical application targeted is flow separation detection. The measurement principle is based on the forced convective heat transfer from a heater element. The sensor structure is composed of three parallel substrate-free wires presenting a high aspect ratio and supported by periodic perpendicular SiO2 micro-bridges. This hybrid structure takes advantages from both conventional hot-films and hot-wires, ensuring near-wall and non-intrusive measurement, mechanical toughness and thermal insulation to the bulk substrate, and it allowed to add the calorimetric sensor functionality to detect simultaneously the wall shear stress amplitude and direction. The central wire is made of a multilayer structure composed of a heater element (Au/Ti) and a thermistor (Ni/Pt/Ni/Pt/Ni) enabling measurement of the heater temperature and a layer of SiO2 between them for electrical insulation. The upstream and downstream wires are thermistors enabling operation in the calorimetric mode. This design provides a high temperature gradient and a homogeneous temperature distribution along the wires. The sensor operates in both constant current and constant temperature modes, with a feedback on current enabled by uncoupling heating and measurement. Welded on a flexible printed circuit, the sensor was flush mounted on the wall of a turbulent boundary layer wind tunnel. The experiments, conducted in both attached and separated flow configurations, quantify the sensor response to a bi-directional wall shear stress up to 2.4 Pa and demonstrate the sensor ability to detect flow separation.

1. Introduction

Active flow control systems are developed to promote air safety, reduce energy consumption or increase aircraft efficiency. A potential candidate for applying flow control strategy is flow separation which is mostly unwanted for many applications and even dangerous in aviation. It can increase drag and energy losses and decrease lift. The measurement of wall shear stress is thereby needed for identifying the location of this phenomenon for implementing a control strategy ([1,2]). For a Newtonian fluid like air, the shear stress τ in a 2D-flow is given by Eq. (1):

$$\tau = \mu \cdot \left(\partial u/\partial y\right)_{wall} \quad (1)$$

where μ is the air dynamic viscosity, u is the flow velocity parallel to the wall, and y is the axis normal to the wall as defined in Fig. 1(a). Fig. 1 illustrates two main kinds of flow separation: the boundary layer separation due to an adverse pressure gradient occurring on a surface with no sharp edges in (a), and another one due to a geometrical obstacle (cavity, obstacle, sharp edges...) in (b).

On an airfoil-like surface like in Fig. 1(a), it is known that an adverse pressure gradient can produce a separation of the boundary layer by decreasing the velocity gradient at the wall and consequently decreasing the friction, before the separation, and creating a back-flow in a separation bubble. In the case (b) flow separation is due to a geometrical obstacle that leads by construction to a

* Corresponding author at: Univ. Lille, CNRS, Centrale Lille, ISEN, Univ. Valenciennes, UMR 8520—IEMN, LIA LICS/LEMAC, Lille F-59000, France.
E-mail addresses: cecile.ghouila@onera.fr (C. Ghouila-Houri), abdelkrim.talbi@iemn.univ-lille1.fr (A. Talbi).

http://dx.doi.org/10.1016/j.sna.2017.09.030
0924-4247/

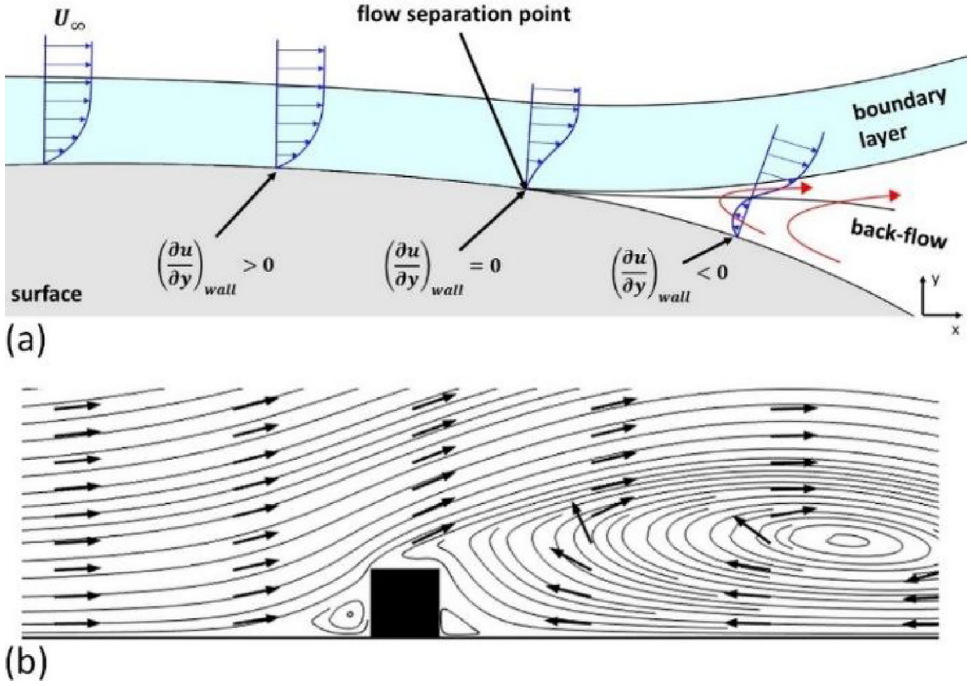

Fig. 1. (a) Schematic of a flow separation on an airfoil like surface (b) A geometry-based separation.

separation bubble [3]. As shown on Fig. 1 and according to Eq. (1), the wall shear stress, and particularly its direction, is directly linked with the flow separation phenomena and its measurement is a key point to detect the state of the flow, either attached or separated.

When measuring fluctuating quantities in high Reynolds number turbulent boundary layers, wall shear stress sensors have to resolve both small length- and velocity-scales at high frequencies, in the view of Kolmogorov scales [4]. Therefore the need of very small, fast and highly sensitive measurement devices can be fulfilled by Micro-Electro-Mechanical Systems (MEMS) technology [5]. Although the present paper does not tackle the fluctuations issue, it must be underlined that the technology presented here will be, in the future, a good candidate for unsteady measurements at such small scales.

Micro-machined flow sensors can be divided into two groups, based on different measurement methods: 'direct' measurement or 'indirect' measurement [6]. For direct measurement of wall shear stress, sensors usually use a floating element that is displaced laterally by the tangential viscous forces in the flow. This displacement implies a variation of an electrical parameter. For instance, in [7] the authors developed a capacitive wall-shear stress sensor with the floating element displacement implying a capacitive variation, reflected in an electric potential variation; the authors in [8] simulated a cantilever-based flow sensor using the piezoresistance effect; and authors in [9] designed and manufactured capacitive airflow sensors based on out-of-plane cantilevers. These sensors present the clear advantage of a direct wall shear stress measurement. However, the necessary floating element implies an electro-mechanical coupling which is sensitive to vibrations. With miniaturization, the mechanical resonance frequency comes close to the vibrations of the measured system structure, in case of moving structures like vehicles. Vibrations affect at least the measure but can also affect the sensor integrity. For avoiding these drawbacks, indirect wall shear stress measurements were developed with various methods. For example, micro-fences using a cantilever structure and piezoresistors are presented in [10]; the exploitation of optical resonances such as whispering gallery modes of dielectric microspheres is proposed in [11] (for which the optical resonance shifts with radial deformations of the spheres due to the shear stress); the deflection of micro-pillars is presented in [12] and thermal-based sensors are presented in the next paragraphs of the present paper. The physical principle used in thermal sensors consists of taking advantage of the convective heat transfer between an electrically heated resistor and a surrounding cooler fluid [6]. As they do not involve a mechanical moving part, thermal flow sensors are widely adopted when dealing with fluid dynamics including laminar or turbulent flows.

Two main kinds of thermal sensors for velocity and wall shear stress have been developed: hot-wire and hot-film sensors. The difference between them lies in the designed structure: in hot-wire sensors the wire resistor is free from the substrate, fixed by two prongs and placed within the flow. On the other side, the wire of hot-film sensors is deposited on a substrate and placed on a surface adjacent to the flow. Hot-wire sensors therefore enable heating uniformity and high sensitivity ([13–15]) but they are fragile and 3D thermal effects occur at the ends of the wire. On the contrary, hot-film sensors are very robust despite their operational constraints. In particular, they suffer from heat losses through the substrate on which the wire is deposited. Various materials have thus been used to increase thermal insulation such as silicon nitride [16], glass [17] or a flexible polymer ([18–20]). These sensors, which are easy to mount flush to the wall, are often used for detecting flow separation and for wall shear stress measurement. To improve the performance (sensitivity and time response) of hot-film sensors, the heat losses need to be reduced and bulk-machining techniques enable the deposition of the wire on a cavity-backed membrane [21].

This paper presents a thermal wall shear stress sensor designed to advantage of the best of both hot-film and hot-wire sensors. In the designed structure, the heater and the measurement elements consist of long metallic wires isolated from the substrate and suspended by periodic silicon oxide micro-bridges [22]. This design allows thermal insulation, mechanical toughness and a hot-wire like behaviour, as the wires are within the flow, while ensuring non-intrusive measurement. The first results on this structure were presented in [23], in a micro-channel. Then, as published in 2016,

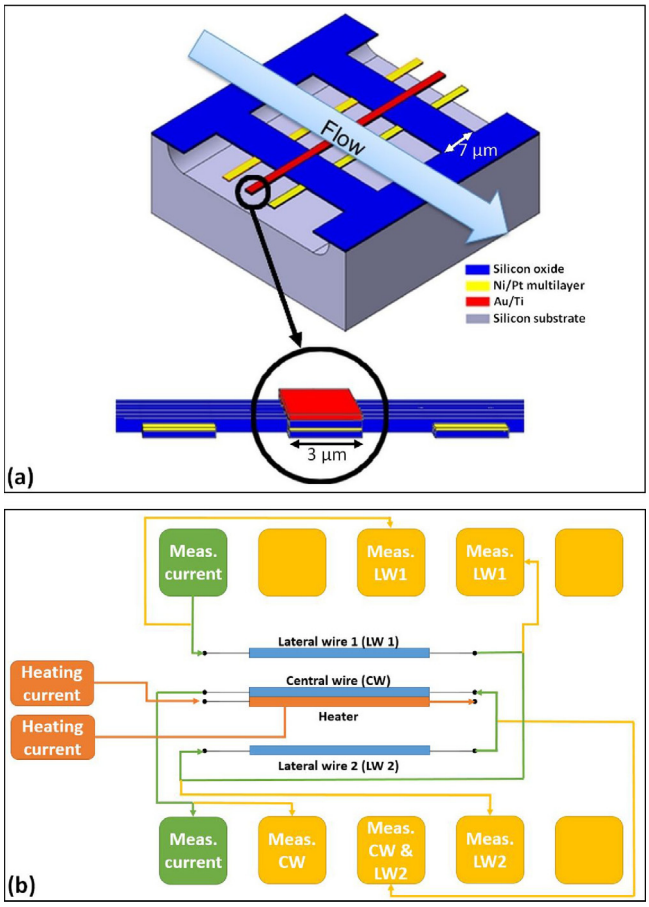

Fig. 2. (a) Schematic of the sensor design (b) Schematic of the sensor wiring (better in color).

an improved design added the detection of the flow direction using the calorimetric principle ([24,25]). This principle exploits the difference of temperature when two other identical sensing elements are placed on both sides of the heater: the flow direction cools differently these elements and a differential measure allows flow direction sensing [26]. In 2017, another group reported a calorimetric sensor for wall shear stress measurement but with a different design [27]. The present paper deals with the same kind of sensor initiated in [25] but targeting more specifically the detection of flow separation. Presented here are all the characterizations performed on the sensor, both electrical and thermal, along with comparisons to numerical studies, and wind tunnel experiments in both attached and separated flows.

2. The thermal MEMS sensor: design and fabrication process

2.1. Design and working principle

The sensitive part of the sensor, presented in Fig. 2(a), consists in three parallel micro-wires, free from the substrate, mechanically supported by silicon oxide micro-bridges over a cavity, and designed to be oriented perpendicular to the flow. The central wire combines heating and wall shear stress measurement as a classical hot-wire. The two other wires, arranged on both sides of the central wire, use the calorimetric principle and are used to detect the flow direction. As they are cooled differently by the flow, the upstream wire being cooler than the downstream one, the temperature difference between them indicates the flow direction.

Table 1
Geometrical parameters of the sensor.

Parameters	Sensing wires	Heater	Brides
Length	1 mm	1 mm	30 µm
Width	3 µm	3 µm	7 µm
Thickness	130 nm	220 nm	500 nm

The geometrical parameters are summarized in Table 1. The wires are 3-µm-wide for 1-mm-long, for a less than one micron thick. Each wire is isolated from the substrate by a 20 µm deep cavity to avoid heat losses by conduction into the substrate and to increase the convective heat transfer. The wires are then within the flow, enabling hot-wire like behaviour while ensuring a non-intrusive measurement. The high aspect ratio of the wires enables a high temperature gradient in the flow direction and a homogeneous temperature profile along the wire. The 32 periodic silicon oxide bridges allow the structure to be mechanically robust despite the wires length. Each micro-bridge is separated from the next one by about 20 µm (Fig. 2(a)). The central wire is multilayer-structured: one layer is the heater, made of Au/Ti, the second one is the measurement wire, a Ni/Pt layer, and a third one of 200-nm-high SiO_2 separates the first two layers, acting as insulator. The heater layer is the only one powered, and it heats the whole sensor structure. The three other Ni/Pt layers are designed for sensing: a 100-µA current is imposed for a resistance measurement using the 4-wires measurement technique. This technique uses four contacts for the measurement of a given resistance, two on both sides of the resistor: one contact on each side for the current supply (100 µA) and the two others for the resistance measurement (Fig. 2(b)). The 4-wires technique allows the measurement of the wire resistance itself without the parasite resistances of the contacts. Measurement and heating are thereby electrically uncoupled to improve the signal to noise ratio and to allow an appropriate material selection. Therefore, the measurement wires are Ni/Pt/Ni/Pt/Ni multilayers reaching about 130 nm height in total. This combination was chosen for its temperature-dependent resistivity, which will be shown below. The heater is mainly comprised of Au (200 nm), a chemically inert material, with good thermal and electrical properties. The Ti layer of 20 nm is an adhesion layer.

A 3D finite-element simulation was performed using COMSOL Multiphysics with the Heat transfer in fluids and solids module, to study the sensor working behaviour. The simulated cell corresponds to an 80-µm-long part of the sensitive structure, with three micro-bridges (Fig. 3(a)), but with boundary conditions fixed such that the cell can be considered infinitely duplicated. The transversal length of the computation domain is 120 µm long. The temperature of the substrate walls is fixed at the initial one, and the heater is heated with a constant power. Additionally, the mesh is unstructured in COMSOL computation, and is composed of about 3 million elements.

As shown in Fig. 3, when the gold resistor is heated by an electric current, the heat is transferred to the measurement wires and the surrounding fluid. Fig. 3(a) and (b) present the heat distribution in the sensor structure (wires and bridges) and the fluid for a 7 mW heating power. With a low power consumption, an increase of about 67 K is reached.

In Fig. 3(c), the flow cools the structure by forced convection leading to a temperature decrease, and the thermal boundary layer is deformed. The forced convection through air is included into the heat transfer equation via the velocity profile with zero velocity at the wall, modelled using Eq. (2), valid because the velocity field considered is in the linear sublayer region of a boundary layer.

$$u = y \cdot (\tau/\mu) \tag{2}$$

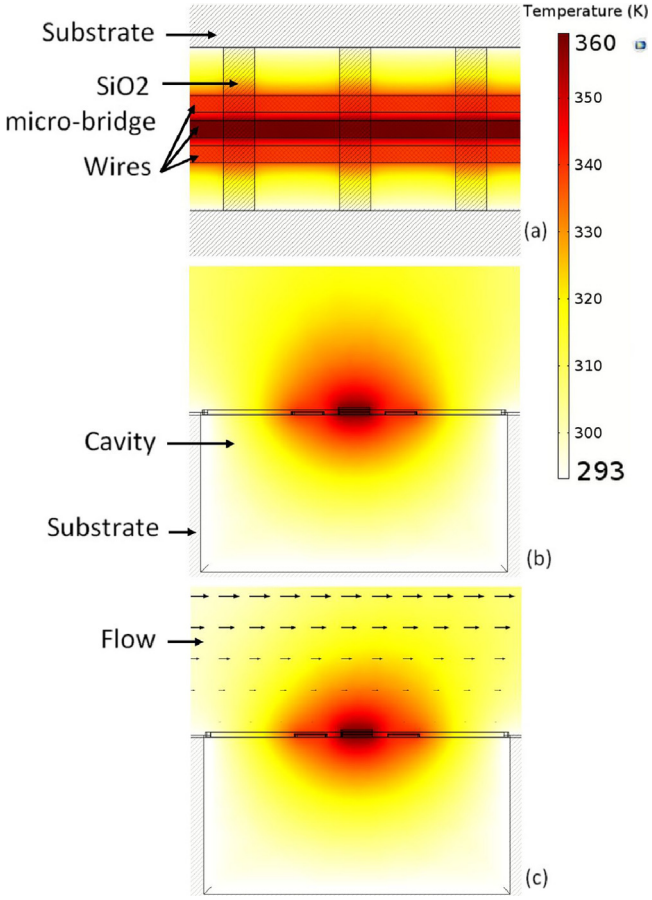

Fig. 3. COMSOL Finite element simulations – Constant power at 7 mW: (a) heat distribution in the wires plane with flow at rest, (b) heat distribution in the plane perpendicular to wires with flow at rest, (c) heat distribution in the plane perpendicular to wires for a wall shear stress of 2 Pa.

2.2. Micro-fabrication and packaging on flexible printed circuit board (PCB)

The micro-machining process was performed on a 3 in (100) silicon wafer for the fabrication of more than one hundred sensors. The detailed process steps are presented in [25]. It contains six main steps and requires four masks. Compared to [25], the thickness of SiO_2 was decreased from 300 nm to 200 nm, the Ni/Pt multilayer deposition was followed by a vacuum annealing to relax mechanical stress and improve stability, and the etch time to release the wire was increased resulting in a deeper cavity. All these modifications were made to enable a higher temperature change and provide higher sensitivity.

Fig. 4(a) and (b) are Scanning Electron Microscopy (SEM) pictures of the manufactured micro-sensor. Fig. 4(a) shows the sensitive part of the sensor (wires and micro-bridges). Fig. 4(b) focuses on the central multi-layered structure (central wire) and distinguishes the various metal layers, which are the heater on top and the measurement wire at the bottom, separated by a dark silicon oxide electrical insulator layer.

The final sensor chip is about 4 mm long by 3 mm wide, the main part of it being occupied by the large front-side pads enabling the electrical contacts recovering at millimeter scale (Fig. 5(a)). The sensor was then welded on a flexible PCB (Fig. 5(b)), using surface mounted component technology, enabling it to adapt to a wind tunnel wall.

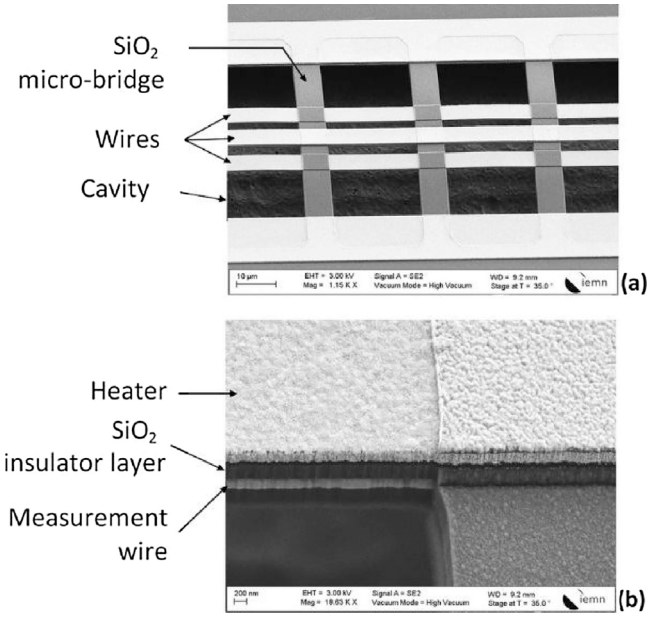

Fig. 4. SEM pictures of the sensor: (a) global structure (b) central wire multilayer structure [24].

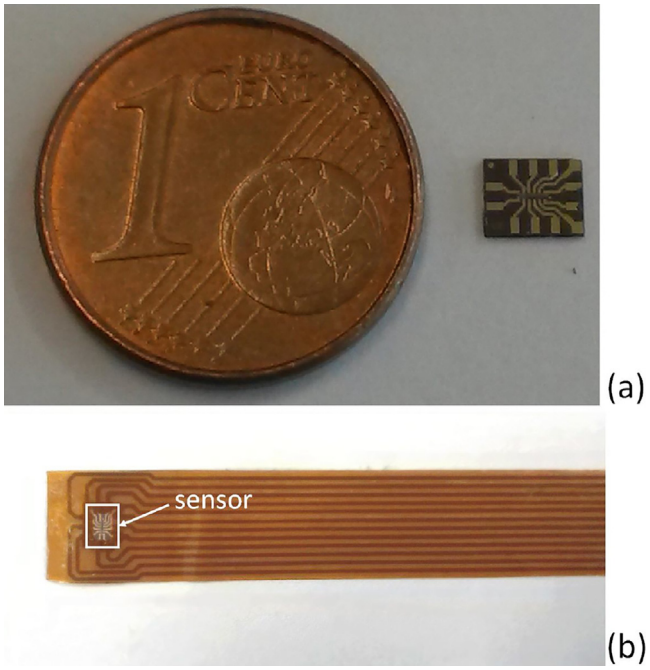

Fig. 5. (a) Sensor chip compared to euro cent (b) Flexible packaging of the sensor.

3. Electrical and thermal response measurements

The first set of measurements were devoted to determinate the Temperature Coefficient of Resistance (TCR) and the temperature elevation with power. The TCR is a material characteristic and is defined by Eq. (3):

$$TCR = \Delta R/(\Delta T \cdot R_0) \quad (3)$$

where R_0 is the resistance of reference at 25 °C, ΔR the resistance variation and ΔT the temperature variation. The measured resistance variation with temperature (Fig. 6) exhibits a linear behaviour between 20 °C and 70 °C resulting in a TCR of about 2380 ± 70 ppm/°C, with the spread of the data measured along the 3 inches

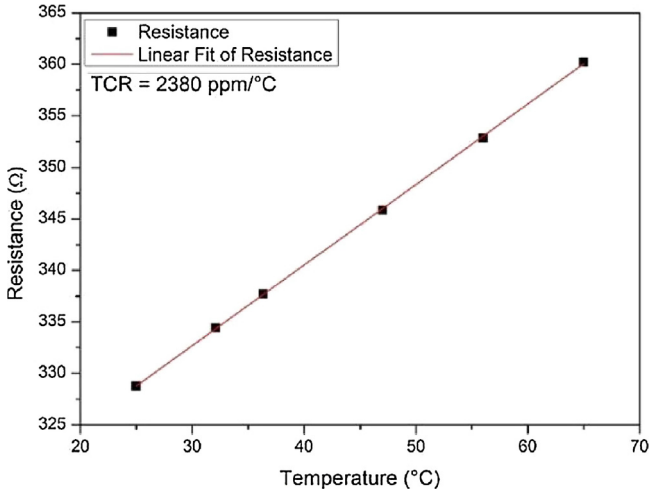

Fig. 6. Pt/Ni/Pt multilayer resistance versus temperature.

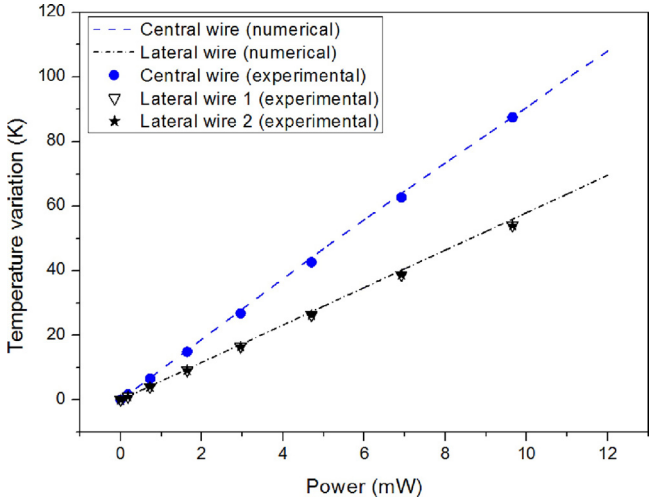

Fig. 7. Electrical characterization (without flow) of the sensor for both central and lateral wires and comparison with numerical results.

diameter wafer. The measured value is smaller than the TCR characteristics of the Nickel bulk material (about 6000 ppm/°C). However, the TCR on thin metallic film highly depends on the thickness of the film and on the deposition technique and is not comparable to bulk material characteristics [28]. The measurement of the TCR is needed to evaluate the temperature of the wire when measuring the resistance.

Next, the temperature elevation by the Joule effect is determined. The measurement setup uses a Keithley 2400 source-meter. Experimental results without flow, compared to numerical ones, are presented on Fig. 7. The numerical results are in agreement with the experimental data. Experimentally the temperature gradient reaches 9.1 ± 0.3 K/mW for the central measurement wire and 5.7 ± 0.4 K/mW for the lateral wires. The lateral wires are indeed isolated from the heater with a 2 μm air gap between them, whereas the central wire is only separated from the heater by 200 nm of silicon oxide, used for electrical insulation and not for thermal insulation.

In order to ascertain the thermal behaviour of our device, thermal imaging is performed using a thermal microscope equipped with an infrared camera (reference MWIR-512 from QFI, 12 × Objective magnification corresponding to 2 μm/pixel). Fig. 8(a) displays the temperature distribution of the heater and the surrounding surface when supplied by a power close to 7 mW.

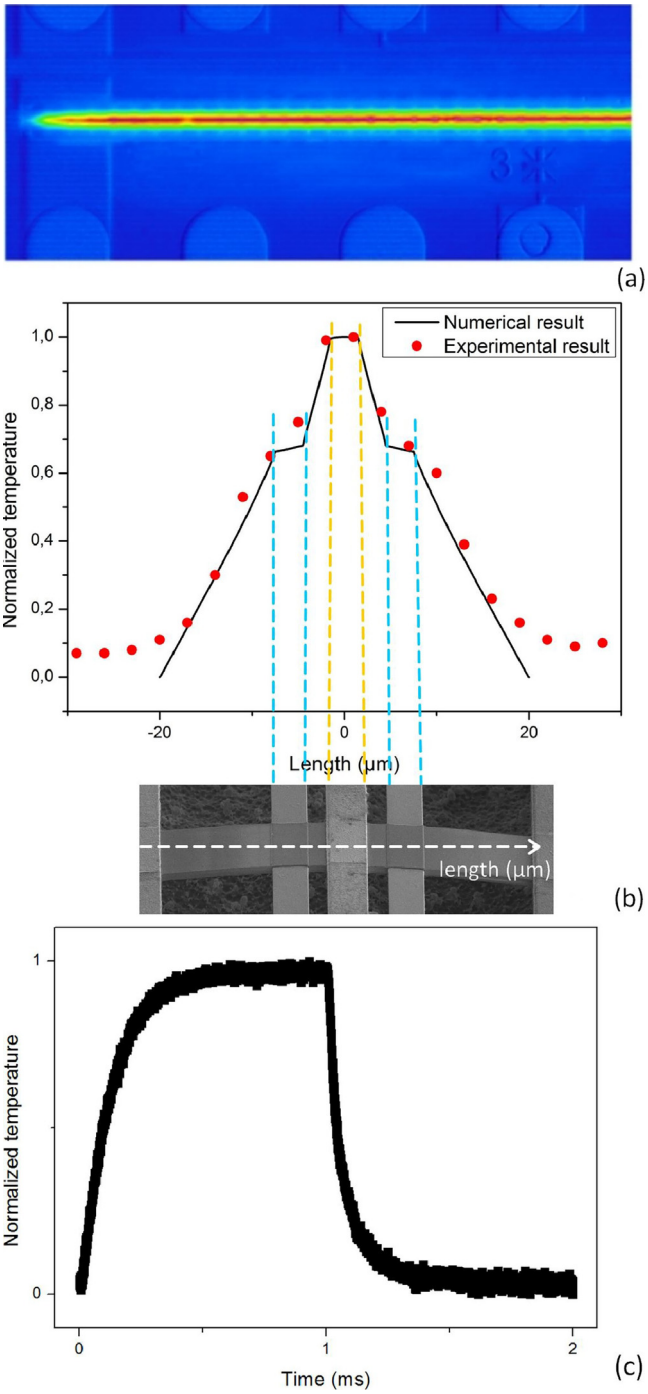

Fig. 8. (a) Thermal camera picture along the length of the manufactured sensor heated with 6 mA current (b) Temperature profile comparison between the experimental and numerical results, perpendicularly to the wires, at the location of a SiO_2 bridge (c) Thermal response time of the sensor.

The micro-bridges structure allows a homogeneous temperature distribution along the wires and a high temperature gradient in the perpendicular direction. The heat distribution is compared to the numerical data on Fig. 8(b) which shows the result for the heat distribution perpendicular to the wires, at the location of a silicon oxide bridge. The experimental and numerical data were normalized by the maximum temperature. The experimental temperature profile is consistent with the simulation. The thermal camera presents also a high-speed mode on a single pixel that was used to evaluate the thermal response time of the sensor (Fig. 8(c)).

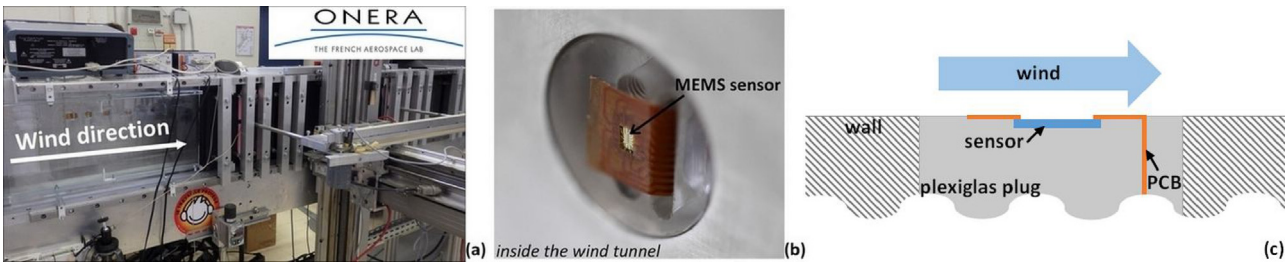

Fig. 9. (a) Turbulent boundary layer wind tunnel in ONERA Lille (b) Flush-mounted IEMN MEMS sensor in the wind tunnel wall (c) Schematic of the sensor-mounting cross-section (scales not respected).

The sensor exhibits a response time at 95 % of 500 μs leading to a bandwidth of 960 Hz when used in constant current mode, similar to the one of a conventional 5 μm diameter tungsten hot wire [29].

4. Wind tunnel experiments for turbulent boundary layer

4.1. Experimental setup

The shear stress measurement by the sensor was tested in a zero-pressure-gradient turbulent boundary layer during a wind tunnel experiment (Fig. 9(a)). The 30 cm x 30 cm test section wind tunnel operates with velocities from 10 m/s to 40 m/s. The flow velocity is measured by a Dantec hot-wire probe, referenced as 55P11, and placed at the center of the test section (15 cm away from the wall). The MEMS sensor is flush mounted at the wind tunnel wall (Fig. 9(b)) using a Plexiglas plug for electrical insulation. Thanks to the flexible packaging, the electrical contacts are recovered outside the wind tunnel, passing by a slot, which is then filled for air tightness. As the contacts are front-side, the sensor is in a small cavity, large enough not to disturb the flow at the sensitive element location (Fig. 9(b) and (c)). A hot-film sensor (Dantec 55R47) is placed at the vicinity of the MEMS sensor, at the same cross section of the wind tunnel, for comparison purposes.

The boundary layer in the wind tunnel was previously characterized with a conventional hot-wire probe mounted on a motorized system allowing displacements normal to the mean flow from the center of the wind tunnel to 0.3 mm from the wall. The velocity profile of the boundary layer enables computation of the experimental momentum thickness θat the MEMS sensor position in the wind tunnel and the corresponding skin friction coefficient C_f, using the relation of Coles-Fernholz developed in [30]:

$$C_f = 2 \cdot \left[\frac{1}{k} \cdot \ln(Re_\theta) + C \right]^{-2} \quad (4)$$

with $k = 0.384$, $C = 4.127$ and $Re_\theta = \left(\theta \cdot U_\infty\right)/\nu$, where U_∞ is the flow velocity at the center of the wind tunnel and ν, the cinematic viscosity. The wall shear stress is linked with the skin friction coefficient by Eq. (5):

$$\tau = \frac{1}{2} \cdot \rho \cdot U_\infty^2 \cdot C_f \quad (5)$$

with ρ being the air density. This method allows to link the hot-wire measurements at the center of the wind tunnel test section with the shear stress at the wall, with an uncertainty less than one-tenth.

4.2. Sensor response to wall shear stress variations

In traditional thermal anemometry, two main operating modes exist: the 'constant current (CC) mode' and the 'constant temperature (CT) mode'. The CC mode, easy to implement, consists in supplying the heater with a constant current. The CT mode regulates the heating current by maintaining the temperature of the wire constant. Here, the sensor can be used in both modes, depending on the application aimed, as presented in this section. Note that the CT mode presents a particularity because the regulation of the heating current in the heater depends on the temperature of the central sensing wire, characterized with a high sensitivity to temperature. The uncoupling between heating circuit and measurement circuit (Fig. 2(b)) enables then a better achievement of the CT mode.

In Fig. 10(a), the sensor was used in CC mode with a 6 mA heating current, corresponding to about a power of 7 mW. The results express the resistance variation ΔR in percent versus the wall shear stress given by Eq. (5) and the velocity profile measurements, for both the central and the lateral wires. ΔR is calculated by Eq. (6):

$$\Delta R(\%) = \frac{(R(7mW, 0Pa) - R(7mW, \tau))}{R(7mW, 0Pa)} \quad (6)$$

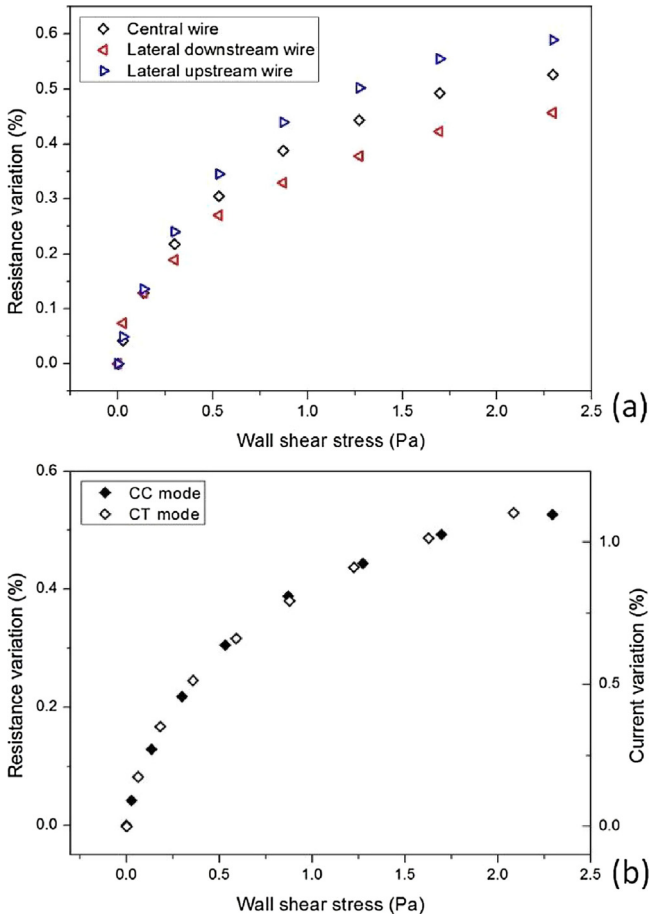

Fig. 10. (a) Measured resistance variations versus wall shear stress for both the central and the lateral wires with the sensor operating in CC mode (b) Calibration comparison between CC and CT modes of operation.

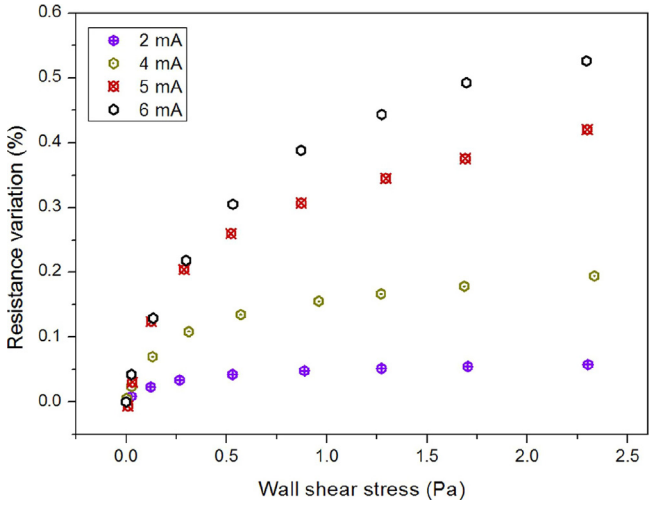

Fig. 11. Measured resistance variations of the central wire versus wall shear stress for different heating currents – sensor used in CC mode.

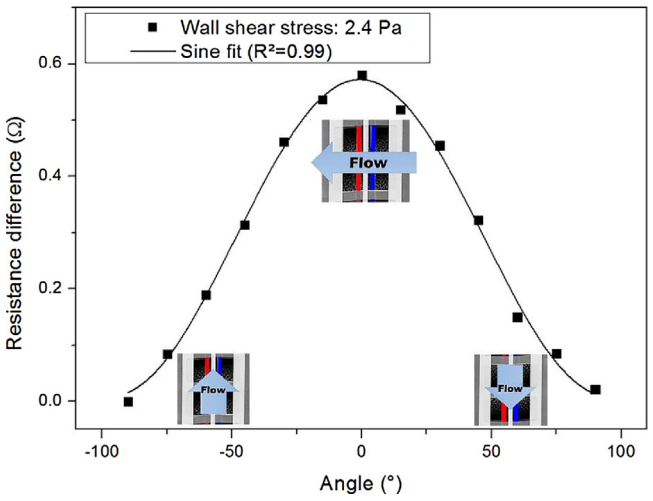

Fig. 12. Measured resistance difference between the two lateral wires versus angle of rotation, for a wall shear stress of 2.4 Pa, and sine fit.

The results in Fig. 10(a) show the measured resistance variations for both the central wire and the lateral wires. As the wires are placed perpendicular to the flow, the lateral wires are distinguished as upstream and downstream the flow. The central wire presents up to 0.53 % of resistance variation for 2.4 Pa while the upstream wire achieves 0.6 % of variation for the same wall shear stress and the downstream wire, only 0.45 %. The lateral wires share the same electrical and thermal characteristics implying that the difference between their variations of resistances is induced by the flow. The wire upstream experiences greater convective cooling by the flow than the downstream one, consistent with a larger resistance variation. Fig. 10(b) presents a comparison between CC and CT modes, considering only the central wire maintained at about 65 °C in CT mode. The sensor presents the same behaviour in both modes but it results in more than 1 % of current variation for a shear stress of 2.4 Pa. The relationship between the wall shear stress τ and the output *s*of the sensor – the resistance variation in CC mode or the current variation in CT mode – fits a fourth order polynomial (Eq. (7)), presenting a similar behaviour as conventional hot-wire sensors.

$$\tau = a_1 s + a_2 s^2 + a_3 s^3 + a_4 s^4 \quad (7)$$

The impact of the heating current on the sensor sensitivity is shown in Fig. 11, in CC mode. As the heating current increased, the sensor sensitivity was improved. Therefore, depending on the aimed application, one can choose to decrease the heating current to save power: for 4 mA, the power consumed is close to 3 mW, whereas for 6 mA the heating power is about 7 mW (cf. Fig. 7).

The Plexiglas plug enables to rotate the sensor allowing angular calibration from −90° to +90°. At 0°, the sensor position corresponds to the one used for the previous experiments, with the sensor wires perpendicular to the flow. This calibration expresses the difference of resistance between the two lateral wires versus the angle of rotation, for a wall shear stress of 2.4 Pa (Fig. 12). The results obtained confirm the sensor sensitivity to the flow direction. However, despite the proper sine fit, with a R-square of 0.99, the sensor presents a small dissymmetry in the values, due to the mounting uncertainty in the rotation.

4.3. Separated flow detection

In [25], flow direction experiments were performed by changing the orientation of the sensor. The results demonstrated the sensor ability to distinguish the flow direction in both orientation, in attached flow situations. Here, the aim is to study the sensor capacity to detect separation and the induced back-flow. This was done by inserting, upstream of the sensor, a 2D step-like obstacle on the wind tunnel wall, as shown in Fig. 13(a) and (b). Two different obstacles heights were considered with respectively 18 mm and 38 mm height. The sensor was flush mounted behind the obstacle, inside the recirculation region: not too far from the obstacle, less than 3 times the obstacle height, nor too close, to remain out of the marginal eddy close to the obstacle. The results are presented in Fig. 14. On all results, the "attached" case corresponds to the flat plate configuration, where there are forward-flow conditions, for reference. The upstream flow velocity is taken at the entrance of the test section, in the middle of the test section. Fig. 14(a) is the response of the central wire of the sensor indicating the wall shear stress amplitude. Fig. 14(b) is the response of the lateral wires

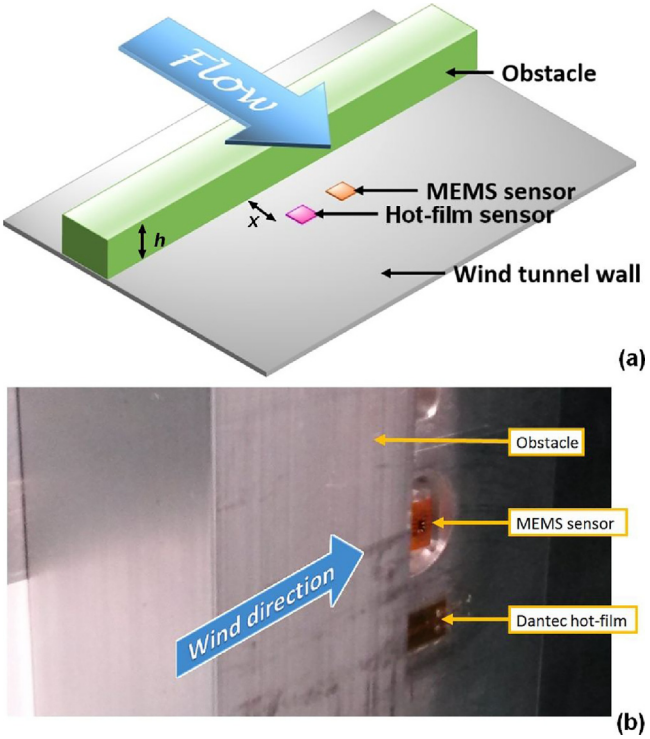

Fig. 13. (a) Schematic of the obstacle experiment set up (b) Picture of set up in the wind tunnel.

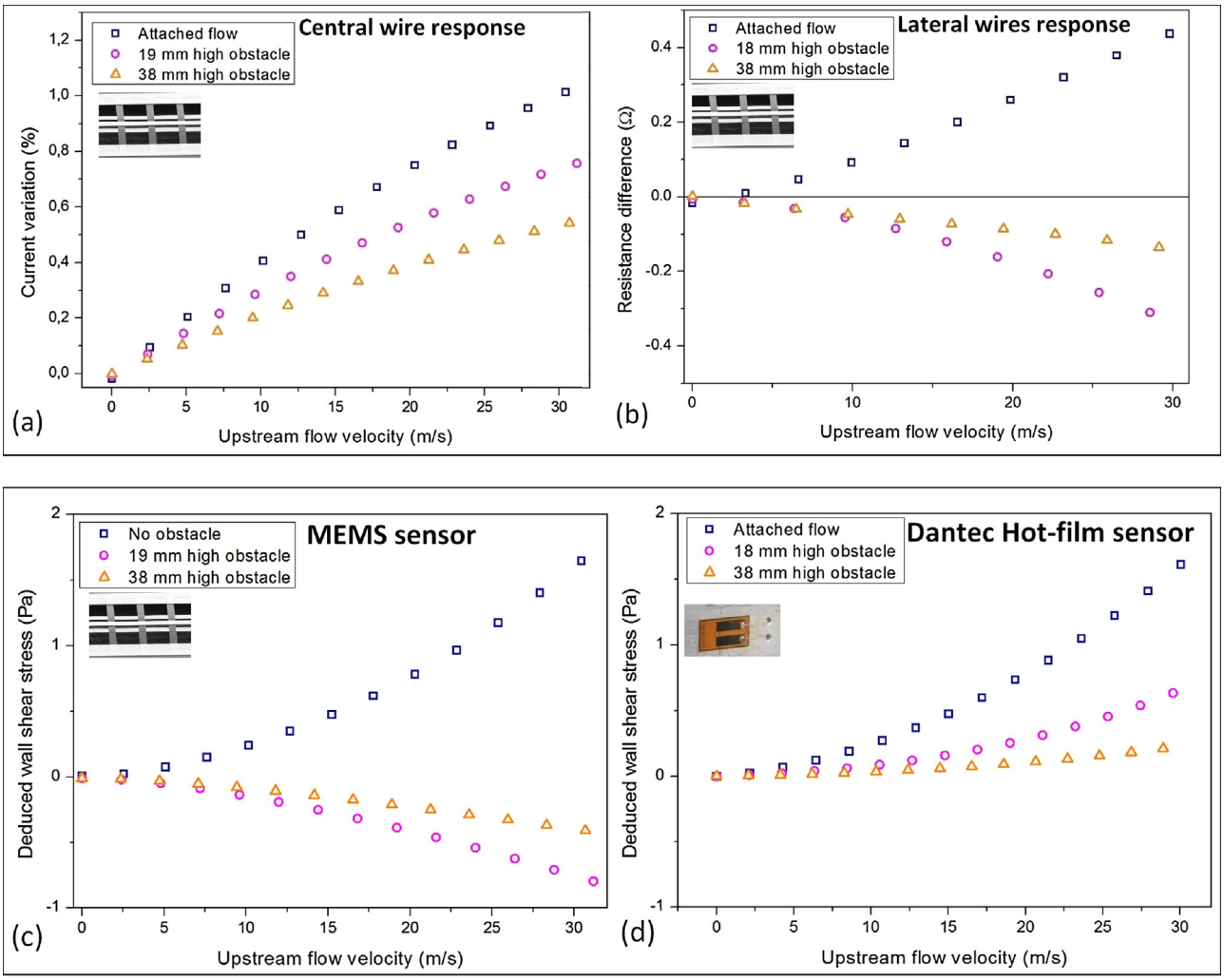

Fig. 14. MEMS sensor response to separation in comparison with flat plate attached flow: (a) Response of the central wire; (b) Response of the lateral wires difference; Deduced wall shear stress in these situations: (c) from the MEMS sensor; (d) from the Dantec hot-film sensor.

indicating the wall shear stress sign. Fig. 14(c) is the deduced wall shear stress from information given by both the central wire and the lateral wires. Fig. 14(d) is the wall shear stress deduced from the Dantec hot-film.

The behaviour of the MEMS sensor in attached (flat plate case) and separated (obstacles case) flow configurations is studied with the sensor used in CT mode (65 °C, 7 mW). The amplitude of the central wire response decreases when the flow is separated (Fig. 14(a)). The resistance difference between the two lateral wires, presented in Fig. 14(b), shows the sign inversion in separated flow. This demonstrates the sensor ability to provide simultaneously the modulus of the wall shear stress and its sign, enabling to detect recirculation bubbles due to separations. The deduced wall shear stress versus upstream velocity (Fig. 14(c)) is calculated using the amplitude of the shear stress (from Fig. 14(a)), coupled with the calibration curve (Fig. 10(b) and Table 2), and its sign (from Fig. 14(b)). For comparison, Fig. 14(d) shows the wall shear stress measured by the Dantec hot-film sensor (CT mode, 120 °C, 100 mW). On both results, the deduced wall shear stress amplitude is gradually less important consistently with the expected flow reversal attenuation when approaching the sensor toward the step from $x/h = 2.3$ (for the 19 mm high obstacle) to $x/h = 0.9$ (for the 38 mm high obstacle), as x and h defined on Fig. 13, while remaining out of the marginal eddy close to the obstacle. The amplitude of wall shear stress measured by the MEMS sensor and the Dantec hot-film sensor is similar. The lateral resistors of the MEMS sensor enables to reveal the inversion of sign of the wall shear stress, unlike the Dantec hot-film sensor, as the flow direction is inversed with separation. The geometry of the obstacles used in the studied configurations leads directly to the flow separation, even at low velocities. The sensor lateral wires reveal this flow property. Moreover, for a given obstacle, the amplitude of the signal response increases (for both the central and the lateral wires) as the velocity increases. This result is consistent with the fact that the recirculation area is strengthened. However, these are preliminary results and visualization techniques, like Particle Image Velocimetry, are needed to fully understand the measurements results. This demonstrates nonetheless the sensor ability to provide simultaneously the modulus of the wall shear stress and its sign, enabling to detect recirculation bubbles due to separations.

Table 2
Calibration constants for the MEMS sensor in both CC and CT modes.

$\tau = a_1 s + a_2 s^2 + a_3 s^3 + a_4 s^4$	CC mode	CT mode
a_1	−0.67254	−0.00713
a_2	19.69283	1.92911
a_3	−65.8641	−1.94176
a_4	87.95425	1.57798
R^2 of the 4th order polynomial fit	0.997	0.999

5. Conclusion

Design, numerical simulations, fabrication, electro-thermal characterizations and wind tunnel experiments results of a novel hot-wire based wall shear stress sensor were presented in this paper. The design is a compromise between conventional hot-wires and hot-films sensors, taking advantages from both structures, as it consists in free hot-wires supported by silicon oxide micro-bridges. The sensor experiences a high temperature gradient, up to 9 °C/mW and a high sensitivity to wall shear stress with up to 0.5 % of resistance variation for 2.4 Pa in CC mode, and more than 1 % of current variation in CT mode. It was also able to detect the sign of the stress due to its 3-wires based design. Experiments conducted in attached and separated flow situations demonstrated the capacity of the sensor to detect separation. In separated flow, the sensor detected the reduction of the wall shear stress modulus and its sign. Further characterizations will investigate the dynamical behaviour of the sensor for detecting shear stress fluctuations in unsteady flows. Then, further work, on a flap model similar to the one used in [2], will perform a flow control using the presented MEMS sensors in unsteady situation. This work will take advantage of this technology for open and closed-loop control strategies.

Acknowledgments

The French National Research Agency (ANR) in the framework of the ANR ASTRID “CAMELOTT” Project funded this work. It was supported by the regional platform CONTRAERO in the framework of the CPER ELSAT 2020 Project, co-financed by the European Union with the European Regional Development Fund and the French State and the Hauts de France Region. The authors also thank RENATECH, the French national nanofabrication network, and FEDER.

References

[1] Gad-el-Hak, Flow control: the future, J. Aircr. 38 (3) (2001) 402–418.
[2] T. Chabert, J. Dandois, É. Garnier, Experimental closed-loop control of separated-flow over a plain flap using extremum seeking, Exp. Fluids 57 (March (3)) (2016).
[3] H. Sturm, G. Dumstorff, P. Busche, D. Westermann, W. Lang, Boundary layer separation and reattachment detection on airfoils by thermal flow sensors, Sensors 12 (October (11)) (2012) 14292–14306.
[4] V. Chandrasekaran, A. Cain, T. Nishida, L.N. Cattafesta, M. Sheplak, Dynamic calibration technique for thermal shear-stress sensors with mean flow, Exp. Fluids 39 (July (1)) (2005) 56–65.
[5] L. Löfdahl, M. Gad-el-Hak, MEMS applications in turbulence and flow control, Prog. Aerosp. Sci. 35 (February (2)) (1999) 101–203.
[6] L. Löfdahl, M. Gad-el-Hak, MEMS-based pressure and shear stress sensors for turbulent flows, Meas. Sci. Technol. 10 (8) (1999) 66.
[7] V. Chandrasekharan, J. Sells, J. Meloy, D.P. Arnold, M. Sheplak, A microscale differential capacitive direct wall-shear-stress sensor, J. Microelectromechan. Syst. 20 (June (3)) (2011) 622–635.
[8] P. Chen, Y. Zhao, Y. Li, Fluid structure interaction analysis and simulation of micromachined cantilever-based flow sensor in Nano/Micro Engineered and Molecular Systems (NEMS), 2014 9th IEEE International Conference on (2014) 350–353.
[9] N. André, B. Rue, G. Scheen, D. Flandre, L.A. Francis, J.-P. Raskin, Out-of-plane MEMS-based mechanical airflow sensor co-integrated in SOI CMOS technology, Sens. Actuators Phys. 206 (2014) 67–74.
[10] T. von Papen, U. Buder, H.D. Ngo, E. Obermeier, A second generation MEMS surface fence sensor for high resolution wall shear stress measurement, Sens. Actuators Phys. 113 (July (2)) (2004) 151–155.
[11] T. Ioppolo, U.K. Ayaz, M.V. Otugen, Performance of a micro-optical wall shear stress sensor based on whispering gallery mode resonators, 47th AIAA Aerospace Sciences Meeting (2009).
[12] S. Große, W. Schröder, Dynamic wall-shear stress measurements in turbulent pipe flow using the micro-pillar sensor MPS3, Int. J. Heat Fluid Flow 29 (June (3)) (2008) 830–840.
[13] A. Talbi, L. Gimeno, J.-C. Gerbedoen, R. Vard, A. Soltani, V. Mortet, V. Preobeazhensky, A. Merlen, P. Pernod, A micro-scale hot wire anemometer based on low stress (Ni/W) multi-layers deposited on nano-crystalline diamond for air flow sensing, J. Micromech. Microeng. 25 (December (12)) (2015) 125029.
[14] P. Pernod, L. Gimeno, A. Talbi, A. Merlen, R. Vard, V. Mortet, A. Soltani, V. Preobeazhensky, ‘Hot-wire sensor of submillimeter size and associated method of production’, FR2958754 (A1) 2011-10-14 WO2011128828 (A1) 2011-10-20 FR2958754 (B1) 2012-10-26 EP2561369 (A1) 2013-02-27 US2013125644 (A1) 2013-05-23 JP2013527436 (A) 2013-06-27 US8978462 (B2) 2015-03-17 EP2561369 (B1) 2015-04-01 DK2561369 (T3) 2015-07-06 JP5770828 (B2) 2015-08-26, 2011.
[15] Y. Fan, G. Arwatz, T.W. Van Buren, D.E. Hoffman, M. Hultmark, Nanoscale sensing devices for turbulence measurements, Exp. Fluids 56 (July (7)) (2015).
[16] E. Vereshchagina, R.M. Tiggelaar, R.G.P. Sanders, R.A.M. Wolters, J.G.E. Gardeniers, Low power micro-calorimetric sensors for analysis of gaseous samples, Sens. Actuators B Chem. 206 (2015) 772–787.
[17] Y. Zhu, M. Qin, J. Huang, Z. Yi, Q.-A. Huang, Sensitivity improvement of a 2D MEMS thermal wind sensor for low-Power applications, IEEE Sens. J. 16 (June (11)) (2016) 4300–4308.
[18] J.J. Miau, T.S. Leu, J.M. Yu, J.K. Tu, C.T. Wang, V. Lebiga, D. Mironov, A. Park, V. Zinovyeg, K.M. Chung, Mems thermal film sensors for unsteady flow measurement, Sens. Actuators Phys. 235 (November) (2015) 1–13.
[19] T.S. Leu, J.M. Yu, J.J. Miau, S.J. Chen, MEMS flexible thermal flow sensors for measurement of unsteady flow above a pitching wind turbine blade, Exp. Therm. Fluid Sci. 77 (2016) 167–178.
[20] M. Shikida, K. Yoshikawa, S. Iwai, K. Sato, Flexible flow sensor for large-scale air-conditionning network systems, Sens. Actuators A Phys. 188 (2012) 2–8.
[21] I. Haneef, M. Umer, M. Mansoor, S. Akhtar, M.A. Rafiq, S.Z. Ali, F. Udrea, A tungsten based SOI CMOS MEMS wall shear stress sensor, IEEE SENSORS Proceedings (2014) 1475–1478.
[22] R. Viard, A. Talbi, P. Pernod, A. Merlen, and V. Preobrazhensky, ‘Miniaturised Sensor Comprising A Heating Element, And Associated Production Method’, FR2977886 (A1) 2013-01-18 WO2013008203 (A2) 2013-01-17 WO2013008203 (A3) 2013-03-07 CN103717526 (A) 2014-04-09 EP2731908 (A2) 2014-05-21 US2014157887 (A1) 2014-06-12 EP2731908 (B1) 2015-09-09 DK2731908 (T3) 2015-12-21, 2013.
[23] R. Viard, A. Talbi, P. Pernod, A. Merlen, C. Frankiewicz, J.-C. Gerbedoen, V. Preobrazhensky, A robust thermal microstructure for mass flow rate measurement in steady and unsteady flows, J. Micromech. Microeng. 23 (June (6)) (2013) 65016.
[24] C. Ghouila-Houri, J.-C. Gerbedoen, J. Claudel, Q. Gallas, E. Garnier, A. Merlen, R. Viard, A. Talbi, P. Pernod, Wall shear stress and flow direction thermal MEMS sensor for separation detection and flow control applications, Procedia Eng. 168 (2016) 774–777.
[25] C. Ghouila-Houri, J. Claudel, J.-C. Gerbedoen, Q. Gallas, E. Garnier, A. Merlen, R. Viard, A. Talbi, P. Pernod, High temperature gradient micro-sensor for wall shear stress and flow direction measurements, Appl. Phys. Lett. 109 (December (24)) (2016) 241905.
[26] J.T.W. Kuo, L. Yu, E. Meng, Micromachined thermal flow Sensors—a review, Micromachines 3 (4) (2017) 550–573.
[27] Q. Weiss, Y. Schwaab, A. Boucetta, C. Giani, P. Guigue, Simulation and testing of a MEMS calorimetric shear-stress sensor, Sens. Actuators Phys. 253 (2017) 210–217.
[28] P.M. Hall, The effect of expansion mismatch on temperature coefficient of resistance of thin films, Appl. Phys. Lett. 12 (6) (1968).
[29] S.C.C. Bailey, G.J. Kunkel, M. Hultmark, M. Vallikivi, J.P. Hill, K.A. Meyer, C. Tsay, C.B. Arnold, A.J. Smits, Turbulence measurements using a nanoscale thermal anemometry probe, J. Fluid Mech. 663 (2010) 160–179.
[30] H. Nagib, K.A. Chauchan, P.A. Monkewitz, Approach to an asymptotic state for zero pressure gradient turbulent boundary layers, Philos. Trans. R. Soc. 365 (2007) 755–770.

Biographies

Cécile Ghouila-Houri received her MS degree in Engineering with specialization in Micro-Nanotechnology, Wave Physics and Telecommunications from Ecole Centrale de Lille in 2015. She began her PhD in November 2015, joining the ONERA, the French Aerospace Lab, and the IEMN, the Institute of Electronics, Microelectronics and Nanotechnology of Lille. Her research concerns microsystems for fluids dynamics applications.

Quentin Gallas, a graduate engineer from ISTIL (Lyon) in 2001, received his MS degree and his PhD in 2005 at the University of Florida. Back to France, he joined the Renault group where he spent 9 years in the field of aerodynamics, using both experimental and numerical tools. In 2014, he joined ONERA, the French Aerospace Lab, in the Aerodynamics Department in Lille center. He is in charge of the Physics of Fluids activities. His areas of study and research cover flow control technologies, development of experimental methodologies and metrology in air and water, and terrestrial and naval aerology.

Éric GARNIER Dr, habilited, E., Garnier, is senior research engineer in the aerodynamics, aeroelasticity and acoustics department of ONERA. He is recognized as an expert in Large Eddy Simulation and flow control. He has contributed to 36 papers in peer-reviewed journals, 58 communications with proceedings and one textbook (LES for compressible flows with N. Adams and P. Sagaut). He has been involved in the supervision of 10 PhD Students and 8 master students.

Alain MERLEN Professor Emeritus at Lille University, Alain Merlen is a former chief scientist of the fluid mechanics and energetic branch at ONERA, The French national aerospace research centre, from 2012 to 2015. He is an expert for different French research evaluation agencies: French ministry of research, French agency of research (ANR), French agency of research evaluation (AERES), and French national commission of universities (CNU). He is an expert for UE and UK Programs too. He supervised 23 PhDs, and he is author and co-author of 56 papers in peer review papers and 5 patents. He won 2 awards. He is a member of a NATO scientific Panel and a former Chaiman of the French academic society of mechanics (AUM).

Romain Viard received his MS degree in Engineering with specialization in Micro-Nanotechnology, Wave Physics and Telecommunications from Ecole Centrale de Lille in 2006 and his PhD degree in 2010 from Ecole Centrale de Lille and the IEMN UMR CNRS 8520. He is currently at the Head of Innovation in Thurlemec Company in Pulversheim and CEO of Fluiditech. His field of research concerns the development of innovative solutions for the manipulation and the measure of fluidic systems.

Abdelkrim Talbi is Associate Professor at Centrale Lille and researcher at IMEN UMR CNRS 8520 Institute. He is a member of the International Laboratory on Critical and Supercritical phenomena in functional electronics, acoustics and fluidics (formerly LIA LICS- LEMAC). He received the MS degree in plasma, optics, electronics, and microsystems from the Universities of Metz, Nancy I, and SupElec Metz, in 2000, and the PhD degree in 2003 (LPMIA) from the university of Nancy I. Researches of interest are invention, design, fabrication, characterization, and optimization of micro and nano electromechanical system (MEMS/NEMS): 1- micro-actuators (active materials), 2- micro-acoustic waves and resonant MEMS physical and bio sensors. 3- Micro-acoustic phononic crystals for sensors and microwaves applications. He has authored or coauthored of over 70 refereed publications and he is listed as co-inventor of 4 patents.

Philippe Pernod received the Engineering Degree from Centrale Lille (1986), and the MS degree in ultrasound and imaging (1986), Ph.D. degree in Electronics (1989) and the Doctorat es-Sciences (1996) from University of Valenciennes. He is currently Full Professor at Centrale Lille, Head of the AIMAN-FILMS research group of Institute of Electronics, Microelectronics and Nanotechnology and Head on french side of the International Laboratory LICS in functional electronics, acoustics and fluidics. His research interests include Nonlinear magnetoacoustics, Active multiferroic nanostructures, functional electronics, Micro-Magneto-Electro-Mechanical-Systems for sensors, actuators, microfluidics and RF devices, Nonlinear Ultrasonic imaging for the characterization of complex media and flows.